Sea Spray and Its Feedback Effects: Assessing Bulk Algorithms of Air–Sea Heat Fluxes via Direct Numerical Simulations

TIANZE PENG AND DAVID RICHTER

Department of Civil and Environmental Engineering and Earth Sciences, University of Notre Dame, Notre Dame, Indiana

(Manuscript received 24 September 2018, in final form 20 March 2019)

ABSTRACT

Sea spray exchanging momentum, heat, and moisture is one of the major uncertainties in modeling air–sea surface heat fluxes under high wind speeds. As a result of several untested assumptions in existing models and low fidelity in the measurements, questions regarding the appropriate method for modeling the effects of spray on air–sea fluxes still exist. In this study, we implement idealized direct numerical simulations (DNS) via an Eulerian–Lagrangian model to simulate spray droplets in turbulent flows. Then, we verify the bulk spray models of Fairall et al. and Andreas et al. with the detailed physics from DNS. We find that the quality of the underlying assumptions of bulk models is sensitive to the time scales governing spray microphysics and lifetime. While both models assume that spray experiences a uniform and steady ambient condition, our results show that this assumption only works well for droplets with long thermodynamic time scales and relatively short lifetime. When the thermodynamic time scales are short, the models fail to predict the correct temperature and radius change of spray (e.g., condensation), thus spray-mediated heat fluxes, which in turn overestimates the total heat fluxes. Moreover, using our two-way coupled simulations, we find a negative feedback induced by the spray evaporation that may be missing in the bulk models, which could lead to further overestimates of the total heat flux when the spray-mediated flux is treated as an add-on to the corresponding interfacial flux. We further illustrate that the feedback effects are consistent under different flow Reynolds numbers, which suggests that the findings are relevant at practical scales.

1. Introduction

Quantifying and parameterizing the complex physics associated with spray droplets in the high-wind boundary layer has been investigated for decades across various scales, but the degree to which spray mediates air–sea transfer remains in question despite its potential impacts on meteorological forecasting (Wang et al. 2001; Andreas and Emanuel 2001; Soloviev et al. 2014). As noted by Kepert et al. (1999) and others, two fundamental issues need to be solved to fully quantify the effects of spray: 1) the generation mechanisms of spray (i.e., constraining the source function) and 2) the feedback mechanism by which spray droplets modify the local turbulent environment. These issues persist due to the inherent complexity of the system and difficulties in direct observation. The current study focuses on the latter of the two challenges, in particular, the thermodynamic feedback of spray on latent and sensible heat fluxes.

When spray is present, the total (sensible and latent) heat transported from the sea to the air consists of two routes: interfacial fluxes and spray-mediated fluxes (Andreas 1992). It is commonly assumed that these two independent components can be summed to produce the total heat flux, or that if one could estimate the interfacial component, the overall spray effects could be measured via the change of the total. In practice, however, decoupling the two routes, or measuring one in the absence of the other, is not trivial and involves significant approximation. Relatively few experimental or observational studies exist that even attempt to measure the total heat fluxes in high winds, and these are generally based on indirect measurements (Wang and Street 1978; Richter and Stern 2014; Bell et al. 2012), laboratory experiments (Komori et al. 2018; Jeong et al. 2012), or direct eddy covariance measurements (Drennan et al. 2007; Zhang et al. 2008). In these studies, it is challenging to conclusively address the role that sea spray plays, and it remains nearly impossible to distinguish between the interfacial and spray-mediated routes, thus neglecting to provide the necessary detail for assessing whether the total heat flux can be decomposed in this way.

Corresponding author: Tianze Peng, tianze.peng.16@nd.edu

DOI: 10.1175/JPO-D-18-0193.1

When developing models to account for the effects of spray, one must consider both the droplet microphysics (Onishi et al. 2016) as well as the feedback effect of spray onto the surrounding flow. The numerous numerical/theoretical spray models that exist can be categorized into three major groups: bulk algorithms, Eulerian multiphase approaches (or one-dimensional models), and Lagrangian approaches.

Bulk models attempt to estimate the net air–sea fluxes without resolving the corresponding vertical profiles in the atmosphere or the details of spray's dynamics and thermodynamics (Andreas et al. 2015; Bao et al. 2011; Fairall et al. 1994; Mestayer and Lefauconnier 1988). Hence, bulk models are associated with two common hypotheses: 1) contributions from individual sea-spray droplets are independent and can directly add to the interfacial heat fluxes and 2) the sensible and latent heat released from sea spray can be determined from the difference between the initial and final temperature and size of the droplets, neglecting all intermediate dynamics.

However, the question of whether these are reasonable assumptions has not been addressed, which could be the reason for continued discrepancies between measurements and theory. For instance, while some bulk spray models suggest a significant influence of spray droplets on heat fluxes (Andreas et al. 2015), the results from observations (DeCosmo et al. 1996; Drennan et al. 2007; Zhang et al. 2008) and certain experiments (Jeong et al. 2012) indicate a lack of dependence of the heat and moisture transfer coefficients C_H and C_E on wind speed. Other experimental data, however, show that there may be a significant increase in the transfer coefficients due possibly to spray (Komori et al. 2018; Troitskaya et al. 2018a,b). These disagreements show the importance of understanding the details of air-spray turbulent coupling, and the difficulties associated with formulating bulk models and making detailed measurements.

The other two modeling approaches (Eulerian multiphase and Lagrangian) have increased complexity, and attempt to account for the vertical transport of the droplets as they interact with the airflow. In 1D Eulerian models (Rastigejev and Suslov 2016; Bianco et al. 2011; Lighthill 1999; Makin 1998), vertical transport of momentum, heat, and moisture at the air–sea interface (ASI) are modeled via turbulence closure schemes. Spray-mediated heat fluxes are quantified in a similar manner as bulk models, and their influence on the vertical profiles of moisture, temperature, and momentum are treated as a horizontally homogeneous sink/source to the continuum phase (air). Here, the coupling between phases is included, and in principle these models can capture the effects of elevated spray sources on the vertical profiles of air temperature and humidity. Again, however, the assumptions behind calculating the spray source/sinks on energy and moisture require careful investigation and are nearly impossible to measure directly.

Lagrangian spray models individually track spray droplets as well as by stochastically (Mueller and Veron 2014a,b) or deterministically (Edson and Fairall 1994; Edson et al. 1996; Peng and Richter 2017, hereinafter PR17; Druzhinin et al. 2018) assigning background turbulent fields of velocity, temperature, and humidity. The goal of these methods is to better resolve the dynamics of droplets during their lifetime and understand their bulk behavior, albeit with increased computational cost. A trade-off exists in deciding whether to treat the background flow in a simple manner (e.g., one-dimensional Monin–Obukhov theory) or attempting to resolve the turbulence explicitly, and in the former, assumptions must again be made in treating the two-way coupling of heat and moisture between the spray and air phases. To emphasize the physical transport and coupling processes that sea-spray droplets experience at the turbulent ASI, high-resolution Eulerian–Lagrangian simulations are used in this study to assess the assumptions made in bulk models.

In our previous numerical study (PR17), via direct numerical simulation (DNS), we investigated the sensitivity of the modification of sensible and latent heat flux on various spray parameters. In general we found two broad categories of spray size with distinct influences on the total heat fluxes: small droplets (less than roughly 50 μm in diameter) self-limit their amount of enhancement of total heat flux; larger droplets, on the other hand, have the potential to enhance the total heat flux. The self-limiting of the smaller droplets is due to cancellations between sensible and latent spray-mediated fluxes, and its magnitude is relatively insensitive to its concentration. However, the magnitude of the enhancement by larger droplets depends on spray concentration. We further found that these two scenarios could be distinguished quantitatively by droplet response time scales—for example, when droplets cannot achieve temperature equilibrium with the surroundings given their relatively short lifetime, they deposit both sensible and latent heat.

The current study connects idealized but physics-resolving DNS simulations with bulk air–sea models for spray's influence on the total heat flux. We utilize the high-resolution solutions of DNS in idealized, droplet-laden open-channel flows in order to carefully investigate the modeling framework and hypotheses present in two common bulk spray models (Fairall et al. 1994; Andreas et al. 2015). Thus, we try to answer the following scientific questions: Can the spray-mediated heat

flux be directly added to the interfacial heat flux? How significant is the feedback effect of spray droplets? How can one specify effective atmospheric conditions in a simplified bulk model?

2. MethodWhat is the main cause of tornadoes?

a. Overview

The primary aim of this study is to use DNS to directly test certain assumptions made in bulk estimates of spray-mediated thermodynamic fluxes, and in particular those of Fairall et al. (1994) and Andreas et al. (2015). For the bulk models, we simplify the details (e.g., spray generation), and focus instead on the fundamental hypotheses made for the total heat flux and spray microphysics that can be assessed by DNS.

For DNS, we use the same numerical scheme of droplet-laden turbulent flows as our previous study (PR17) that is adapted from Helgans and Richter (2016). We treat turbulent air flows and spray droplets separately. Hence there are two phases in the model: a carrier phase (air) and a dispersed phase (droplets). For the carrier phase, we use the DNS model to resolve turbulence in an open-channel flow. For spray droplets, we compute the dynamics and thermodynamics of each droplet individually from Lagrangian perspective, and treat them as point particles which respond to the local fluid velocity, temperature, and humidity. In this section, we will introduce both the bulk and DNS models as well as the methodology for testing the bulk models using DNS.

b. Bulk parameterizations for spray-mediated heat fluxes

The fundamental concern we address in this study is whether the heat flux can be expressed as the direct sum of interfacial and spray-mediated components. To start, we follow the two bulk models and define the total heat flux H_T that consists of the interfacial (subscript ''int'') and spray-mediated (subscript ''sp'') components. Each term can be further decomposed into their latent (subscript L) and sensible (subscript s) components; that is,

$$H_T = H_{\rm int} + H_{\rm sp} = H_{L,\rm sp} + H_{L,\rm int} + H_{s,\rm sp} + H_{s,\rm int}, \qquad (1)$$

and we list the descriptions for each term in Table 1. Thus, the estimation process for the total flux requires accurate quantification of all four components in Eq. (1) at the air–sea interface. For example, the sensible and latent interfacial heat fluxes can be estimated based on gradient-wind transfer laws of the (potential) temperature and specific humidity

TABLE 1. List of symbols for heat fluxes used in this study.

Variables	Description
H_T	Total heat flux computed by DNS
$H_{s,\rm sp}$	Sensible spray-mediated heat flux computed by DNS
$H_{L,\rm sp}$	Latent spray-mediated heat flux computed by DNS
$H_{s,\rm int}$	Sensible interfacial heat flux computed by DNS
$H_{L,\rm int}$	Latent interfacial heat flux computed by DNS
$\overline{Q}_s^{\langle \rm A15\rangle}$ or $\overline{Q}_s^{\langle \rm F94\rangle}$	Bulk sensible spray-mediated heat exchanging rate (the nominal flux) with the model specified by the superscript (e.g., A15 or F94)
$\overline{Q}_L^{\langle \rm A15\rangle}$ or $\overline{Q}_L^{\langle \rm F94\rangle}$	Bulk latent spray-mediated heat exchanging rate (the nominal flux) with the model specified by the superscript (e.g., A15 or F94)
$\overline{Q}_s$	Estimates of sensible spray-mediated heat exchanging rate (the nominal flux) via Eq. (8) with inputs from DNS
$\overline{Q}_L$	Estimates of latent spray-mediated heat exchanging rate (the nominal flux) via Eq. (9) with inputs from DNS
$\Delta H_{\rm int}$	The change of the total interfacial heat flux of spray-laden DNS simulations from the unladen simulations
ΔH_T	The change of the total heat flux of spray-laden DNS simulations from the unladen simulations

(Andreas et al. 2015; Andreas and Emanuel 2001), which is commonly used among bulk models. However, parameterizing the spray-mediated sensible and latent heat fluxes varies across different bulk models because of different assumptions associated with the spray microphysics.

Specifically, the two common bulk models considered in this study, that of Fairall et al. (1994) (this model will be referred to hereinafter as F94) and that of Andreas et al. (2015) (this model will be referred to hereinafter as A15), estimate spray evaporation differently. F94 assumes that the temperature change will be the only effect that contributes to the total spray-mediated heat flux; that is,

$$H_{\rm sp}^{\langle \rm F94\rangle} = \overline{Q}_s \quad \text{and} \qquad (2)$$

$$H_{L,\rm sp}^{\langle \rm F94\rangle} = \overline{Q}_L, \qquad (3)$$

so that

$$H_{s,\rm sp}^{\langle \rm F94\rangle} = \overline{Q}_s - \overline{Q}_L. \qquad (4)$$

Here in Eqs. (2)–(4), $\overline{Q}_s$ and $\overline{Q}_L$ respectively represent the nominal spray-mediated sensible and latent exchange rates—that is, the rate of net exchange of sensible and latent heat by the droplets between entering and leaving the ocean.

A15 assumes some degree of compensation due to evaporative cooling; that is,

$$H_{L,\mathrm{sp}}^{\langle \mathrm{A15}\rangle} = \alpha \overline{Q}_L \quad \text{and} \tag{5}$$

$$H_{s,\mathrm{sp}}^{\langle \mathrm{A15}\rangle} = \beta \overline{Q}_s - (\alpha - \gamma)\overline{Q}_L, \tag{6}$$

where the fitting coefficients α, β, and γ are determined by observational data given assumptions on $\overline{Q}_s$ and $\overline{Q}_L$. However, A15 explicitly assumes an increase of sensible heat components induced by spray evaporation, so $0 < \gamma < \alpha$ represents the adjustment of interfacial heat fluxes due to the cooling effect of spray evaporation. Therefore, the total spray-mediated heat flux described by A15 is

$$H_{\mathrm{sp}}^{\langle \mathrm{A15}\rangle} = \beta \overline{Q}_s + \gamma \overline{Q}_L. \tag{7}$$

In comparing Eq. (7) with Eq. (2), one notices the equivalent coefficients $(\alpha, \beta, \gamma) = (1, 1, 0)$ in the F94 model, whereas in A15 the three coefficients are given as $(\alpha, \beta, \gamma) = (2.46, 15.15, 1.77)$. Obviously, the difference in the magnitude of coefficients in the two models could eventually lead to very different influences of spray droplets predicted by the bulk models.

One of the factors that contributes to the discrepancy between the two models is the assumed form of the spray sensible and latent heat exchange rates or the nominal fluxes $\overline{Q}_s$ and $\overline{Q}_L$. Written in generic terms, these take the form

$$\overline{Q}_s = -c_p m_{p,0} \Delta T_p (F/A) \quad \text{and} \tag{8}$$

$$\overline{Q}_L = -L_v \Delta m_p (F/A), \tag{9}$$

where ΔT_p and Δm_p are the mean net difference of spray temperature and radius, respectively, between the initial and final condition when entering the water surface. The F is a spray renewal rate at the surface (related to the spray generation function), and A is the horizontal area of interest. Therefore, both $\overline{Q}_s$ and $\overline{Q}_L$ have units of energy per area per time.

In F94, spray is assumed to enter the surface with a temperature equal to the air temperature at the significant wave height T_a after beginning with a temperature equal to that of the sea surface T_s. Thus $\Delta T_p = T_a - T_s$, which implies an instantaneous temperature adjustment of the spray. On the other hand, A15 assumes that the difference $T_a - T_s$ is the maximum potential temperature difference and that ΔT_p is limited by its residence time (τ_f in the original text of A15 and t_L in this paper) so that, for each size of spray, $\Delta T_p = (T_a - T_s)[1 - \exp(-t_L/\tau_T)]$, where τ_T is the thermal response time of spray defined by Eq. (1.4) in Andreas (2005) as the e-folding time of temperature evolution given steady ambient condition.

Similarly for spray evaporation, for the spray's mass change Δm_p, F94 assumes an instantaneous evaporative adjustment to the conditions at the significant wave height, whereas A15 considers the temporal evolution due to an evaporation time scale τ_r [also defined as an e-folding time in Andreas (2005)] that is much longer than τ_T. Using the DNS, we can calculate directly the quantities ΔT_p and Δm_p, and therefore compare with the assumed forms of A15 and F94.

c. *Numerical scheme of direct numerical simulations*

1) Carrier phase solved via DNS

To represent idealized shear-driven turbulence at the ASI, we simulate turbulent open-channel flow driven by a pressure gradient with various boundary conditions. We further assume 1) incompressible flow, 2) neutral stability for the carrier phase, 3) a flat surface at the lower boundary, and 4) constant viscosity and thermal diffusivity. Thus, this system is meant to focus on the physics underlying turbulence-droplet coupling and is not meant to replicate a real air–sea interface. With the above simplifications, the following governing equations describe the conservation of mass, momentum, temperature, and humidity of the carrier phase.

For an incompressible flow, conservation of mass yields a divergence-free velocity field,

$$\frac{\partial u_i}{\partial x_i} = 0, \tag{10}$$

where u_i is the velocity of the air at location x_i, and a pressure Poisson equation is used to enforce Eq. (10). Conservation of momentum is calculated by solving

$$\frac{\partial u_i}{\partial t} + u_j \frac{\partial u_i}{\partial x_j} = -\frac{1}{\rho_a}\frac{\partial P}{\partial x_i} + \nu_a \frac{\partial^2 u_i}{\partial x_j \partial x_j}, \tag{11}$$

where P is the pressure, ρ_a is the air density, and ν_a is the kinematic viscosity of air (see Table 2 for parameter values).

The temperature T and specific humidity q ($=\rho_v/\rho_a$, the ratio of vapor density to the constant dry-air density) of the air are computed via an advection–diffusion equation,

$$\frac{\partial \phi}{\partial t} + u_j \frac{\partial \phi}{\partial x_j} = D_\phi \frac{\partial^2 \phi}{\partial x_j \partial x_j} + \frac{1}{\rho_a} S^\phi, \tag{12}$$

where $\phi = T, q$ represents either temperature T or specific humidity q. For the diffusion term, D_ϕ represents

TABLE 2. Simulation parameters used in DNS with their descriptions and values.

Parameters	Symbols	Values
Schmidt number	Sc	0.615
Prandtl number	Pr	0.715
Density of air	ρ_a	1.1 kg m^{-3}
Density of water	ρ_w	1000 kg m^{-3}
Kinematic viscosity of air	ν_a	1.537×10^{-5} m^2 s^{-1}
Specific heat of air	$c_{p,a}$	1006 J K^{-1} kg^{-1}
Specific heat of water vapor	$c_{p,v}$	1952 J K^{-1} kg^{-1}
Specific heat of liquid water	c_w	4179 J K^{-1} kg^{-1}
Thermal conductivity of air	κ_T	0.024 J K^{-1} m^{-1} s^{-1}
Latent heat of evaporation	L_v	2.44×10^6 J kg^{-1}
Molecular weight of water	M_w	0.018 kg mol^{-1}
Molecular weight of salt	M_s	0.0584 kg mol^{-1}

constant thermal diffusivity α and vapor diffusivity D_v. The thermal diffusivity is defined as $\alpha = \kappa_T/(\rho_a c_{p,a})$, where κ_T is the thermal conductivity of air, and $c_{p,a}$ is the specific heat of air. These diffusivities are specified by the molecular Prandtl ($\mathrm{Pr} = \alpha/\nu_a$) and Schmidt ($\mathrm{Sc} = D_v/\nu_a$) numbers. The source term S^ϕ in Eq. (12) represents the two-way coupling between the droplets and air, S^h for temperature (due to heat exchange between the droplet and air) and S^q for the specific humidity (due to evaporation/condensation of the droplet). We omit the momentum coupling between spray droplets and turbulent flow for simplicity so that we can isolate and emphasize the thermal coupling effects. Detailed expressions of S^h and S^q are documented in Helgans and Richter (2016).

To solve Eqs. (10)–(12) via DNS, we use a pseudospectral discretization in the periodic streamwise (x) and spanwise (y) directions, and second-order finite differences are applied in the wall-normal z direction. A low-storage third-order Runge–Kutta method of integration in time is performed for both phases. We set the friction Reynolds number, $\mathrm{Re}_\tau = u_\tau \delta/\nu_a$, for various turbulence intensities given by the applied pressure gradient, where u_τ is the friction velocity and δ is the domain height.

2) LAGRANGIAN DROPLETS

As discussed in PR17, we employ the Lagrangian point particle approach to calculate the temporal evolution of position, velocity, temperature, and radius of droplets as the turbulent air carries them. We solve the following Lagrangian equations for each droplet.

The evolution of a droplet's position $x_{p,i}$ is computed by

$$\frac{dx_{p,i}}{dt} = v_{p,i}, \tag{13}$$

where $x_{p,i}$ is independent from the grid used to solve the carrier phase and $v_{p,i}$ is the velocity of an individual droplet. We compute $v_{p,i}$ by assuming only two forms of forcing applied on each droplet: hydrodynamic drag (Stokes drag with a small droplet Reynolds number correction; Clift et al. 1978) and gravitational settling g_z:

$$\frac{dv_{p,i}}{dt} = (1 + 0.15\mathrm{Re}_p^{0.687})\frac{1}{\tau_p}(v_{f,i} - v_{p,i}) - g_z\delta_{i3}. \tag{14}$$

In Eq. (14), the particle Reynolds number is defined as $\mathrm{Re}_p = 2r_p|v_{f,i} - v_{p,i}|/\nu_a$ and is $O(1)$ or smaller and $\tau_p = 4\rho_p r_p^2/(18\nu_a\rho_a)$ is the Stokes relaxation time of droplets, which is dependent on the droplet radius r_p and droplet density ρ_p.

The thermodynamic evolution of droplets during evaporation is computed simultaneously. Here, we follow previous work (Andreas 1992; Andreas et al. 1995; Pruppacher and Klett 1996; Mueller and Veron 2010) for capturing the heat and mass transfer between a single droplet and its immediate surroundings [see the full description in Helgans and Richter (2016)].

For spray evaporation/condensation, the evolution of droplet radius r_p is driven by the local difference between the specific humidity of air q_f interpolated to the droplet location and the specific humidity at the droplet surface q_p. This humidity difference drives gain (when $q_f > q_p$) or loss (when $q_f < q_p$) of droplet mass and leads to an equation governing r_p:

$$\frac{dr_p}{dt} = \frac{1}{9}\frac{\mathrm{Sh}_p}{\mathrm{Sc}}\frac{\rho_p}{\rho_a}\frac{r_p}{\tau_p}\frac{\rho_a}{\rho_w}(q_f - q_p), \tag{15}$$

where ρ_w and ρ_a are the density of pure water and air, respectively, and $\mathrm{Sh}_p = 2 + 0.6\mathrm{Re}_p^{1/2}\mathrm{Sc}^{1/3}$ is the Sherwood number (a dimensionless mass transfer coefficient). The specific humidity at the droplet surface q_p is a function of the droplet temperature T_p, the surface curvature, and the droplet salinity (Pruppacher and Klett 1996), and a detailed expression can be found in PR17 or Helgans and Richter (2016).

For the evolution of droplet temperature T_p, both heat convection $\dot{Q}_{\mathrm{conv}}$ and phase change $\dot{Q}_{\mathrm{latent}}$ result in a change of T_p governed by

$$\begin{aligned}\frac{dT_p}{dt} &= \frac{1}{\rho_w V_p c_L}(\dot{Q}_{\mathrm{conv}} + \dot{Q}_{\mathrm{latent}}) \\ &= \left[-\frac{1}{3}\frac{\mathrm{Nu}_p}{\mathrm{Pr}}\frac{c_{p,a}}{c_L}\frac{\rho_p}{\rho_w}\frac{1}{\tau_p}(T_p - T_a)\right] + \left(3L_v\frac{1}{r_p c_L}\frac{dr_p}{dt}\right),\end{aligned} \tag{16}$$

Here, V_p is the volume of the droplet, ρ_p is the density of the saline droplet, ρ_w is the density of pure water,

TABLE 3. Boundary conditions (BC) of DNS simulations. Parameters T_{bot} and T_{top} represent the temperature at the bottom and top boundaries, RH_{bot} and RH_{top} represent relative humidity at the two boundaries, $r_{p,0}$ represents the initial spray size, Φ_m ($=m_w/m_a$) represents the spray mass ratio to the air, and Re_τ represents friction Reynolds number of the domain.

BC groups	T_{bot} (K)	T_{top} (K)	RH_{bot}	RH_{top}	$r_{p,0}$ (μm)	Φ_m	Re_τ
M1	301.15	298.15	100%	90%	20, 25, 45, 75, 125, and 200	1%, 5%, and 10%	300
M2	301.15	301.15	100%	90%	25, 75, and 200	5%	300
M3	301.15	298.15	100%	100%	25, 75, and 200	5%	300
M4	301.15	296.15	100%	90%	25, 75, and 200	5%	300
M5	301.15	298.15	100%	80%	25, 75, and 200	5%	300
M6	298.15	301.15	100%	90%	25, 75, and 200	5%	300
R1	301.15	298.15	100%	90%	25, 75, and 200	1%	700
R2	301.15	298.15	100%	90%	25, 75, and 200	1%	1500

c_L is the specific heat of liquid water, and L_v is the latent heat of evaporation. The particle Nusselt number, describing the rate of heat convection from the particle, is given by the empirical expression $Nu_p = 2 + 0.6Re_p^{1/2}Pr^{1/3}$ (Ranz and Marshall 1952). See Table 2 for the values of the material parameters.

d. Boundary and initial conditions

The current study, rather than replicating a real system, aims to use DNS to test whether the parameterizations of spray properly capture the complex physics. Thus, we adopt the same initial and boundary conditions of the simulations as in PR17. A no-slip bottom surface and a no-stress top boundary are applied for the air phase at bottom and top boundaries, along with periodic boundary conditions on the sides. For the thermodynamic boundary conditions, we specify six different combinations of temperature and humidity in order to represent a wide variety of thermodynamic gradients at the interface. As most spray studies are motivated by the tropical air–sea interface, among these boundary conditions, the baseline case "M1" in Table 3 is set as: a warm and humid lower surface (T_{bot} = 301.15 K and RH_{bot} = 100%) and a cooler and drier upper boundary (T_{top} = 298.15 K and RH_{top} = 90%). Figure 1 provides a schematic of the numerical system.

The system is initialized with a fully developed, horizontally homogeneous turbulent flow field with a random distribution of spray droplets in the domain. We maintain a constant number of spray droplets in the domain by replacing them with the same amount of droplets that hit the lower surface. Each droplet reintroduced to the flow has a random location along the lower surface with random initial velocities perpendicular to the surface to mimic the randomness of the spray injection in the real system. The initial velocities follow a uniform distribution whose maximum gives the δ_{inj} defined in Table 4 as the maximum height that droplets can reach without turbulence (see details in PR17). Therefore, due to inertia and settling effect, spray's mean profiles of streamwise velocity and concentration vary on spray size (see Fig. 2 in PR17 for example). As the turbulence develops, we obtain a statistically steady droplet production flux, which gives a steady mean F (e.g., F ranges from $8 \times 10^3\,s^{-1}$ to $5 \times 10^6\,s^{-1}$ for various spray sizes when Re_τ = 300), and we get steady mean number concentrations above δ_{inj} ranging from $3.176 \times 10^7\,m^{-3}$ for 20-μm droplets to $152.6\,m^{-3}$ for 200-μm droplets.

e. Simulation setup

The goal in the current study is to understand the thermodynamic response of both spray and the air from the perspective of the finest scales and to connect to the parameterizations in bulk spray models. Among all simulations, we maintain a consistent ratio between the droplets and the Kolmogorov scale (the smallest scale of turbulent motions), and we test three different values of Re_τ to ensure that our conclusions are robust with turbulence levels: 300, 700, and 1500.

Previous studies (Mueller and Veron 2014a; Richter and Sullivan 2014) indicate that the dynamics and thermodynamics of spray are related to its size and its ability to change size and temperature. Since the bulk models assume that contributions from each size are independent, we implement monodispersed spray distributions with radii ranging from 20 to 200 μm to investigate how to better parameterize behavior that varies with size. We maintain a constant number of spray droplets that is determined by the initial mass fraction Φ_m ($=m_w/m_a$), defined as the ratio of the water mass to the mass of the air, for each simulation.

Therefore, we target at two types of statistics from DNS as results. First, we investigate the temporal mean of the vertical heat fluxes, and second, we calculate statistics of spray droplets (e.g., residence time, temperature change, etc.). To have temporally converged statistics, we run the simulation for a time of at least $30\delta/u_\tau$, and we then verify that all statistics are converged to within 1%. We list the details of the simulation settings of DNS for each of the three Re_τ in Table 4.

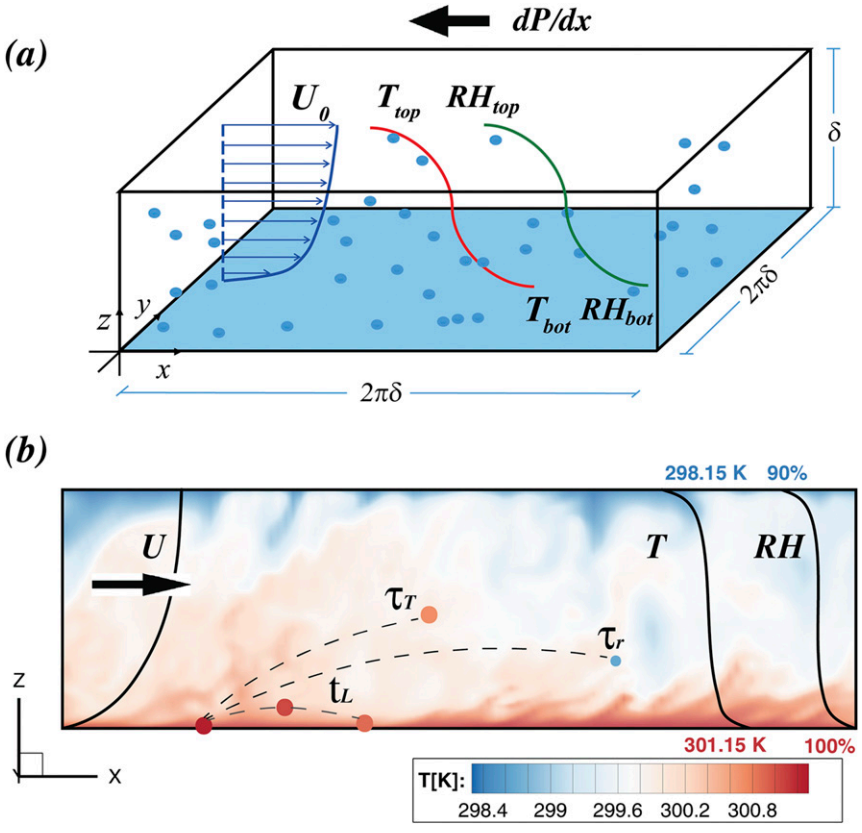

FIG. 1. An overview of the DNS model: (a) a 3D schematic of the computational domain used in DNS, where δ is the height of the domain and other parameters are documented in Table 4, and (b) a schematic showing spray time scales in an x–z cross section of the domain with an instantaneous contour of simulated air temperature (cf. "M1" in Table 3 for boundary conditions). Three time scales listed near dashed lines are the residence time t_L, temperature response time τ_T, and radius response time τ_r.

f. Assessing bulk models via DNS

In our DNS model, the open-channel turbulent flow provides a uniform total vertical heat flux. This constant vertical heat flux is consistent with what bulk models commonly assume and allows for us to compare the two types of models for the thermodynamic coupling between phases and the role of droplet microphysical processes. We compute each component of heat flux found in Eq. (1) explicitly via Eqs. (10)–(16) in DNS. Therefore, we can attempt to reconstruct the DNS-obtained fluxes via the bulk model formulations and provide physical interpretations behind the fitting coefficients. In addition, for the bulk estimation of spray-mediated fluxes, all variables in Eqs. (8) and (9) are known or can be measured from the Lagrangian solutions of DNS.

We first examine the how well F94 and A15 predict the spray-mediated heat fluxes given by Eqs. (2)–(7). Second, we test the magnitude of spray's feedback term (γ term) to predict the total heat flux given only an interfacial heat flux without spray droplets and the mean difference of spray's temperature ΔT_p and radius Δr_p. Third, we will discuss the approximation of ΔT_p and Δr_p as well as spray's overall influence on the total heat flux H_T.

3. Results and discussion

a. Predicting spray-mediated heat fluxes

We start the assessment with the spray-mediated heat fluxes. First, we follow the expressions of F94 via

TABLE 4. Grid setup under different Re_τ. The N_x, N_y, and N_z represent grid numbers in the x, y, and z directions, respectively; g_z is the gravity scaled for the DNS, δ is the dimensional height of the domain, and δ_{inj} is the maximum height that droplets with initial velocity can reach.

Re_τ	N_x	N_y	N_z	g_z (m s^{-2})	δ (m)	δ_{inj} (mm)
300	128	256	128	0.8027	0.04	5.000
700	256	512	256	1.0302	0.08	4.286
1500	512	1024	512	1.1398	0.16	4.008

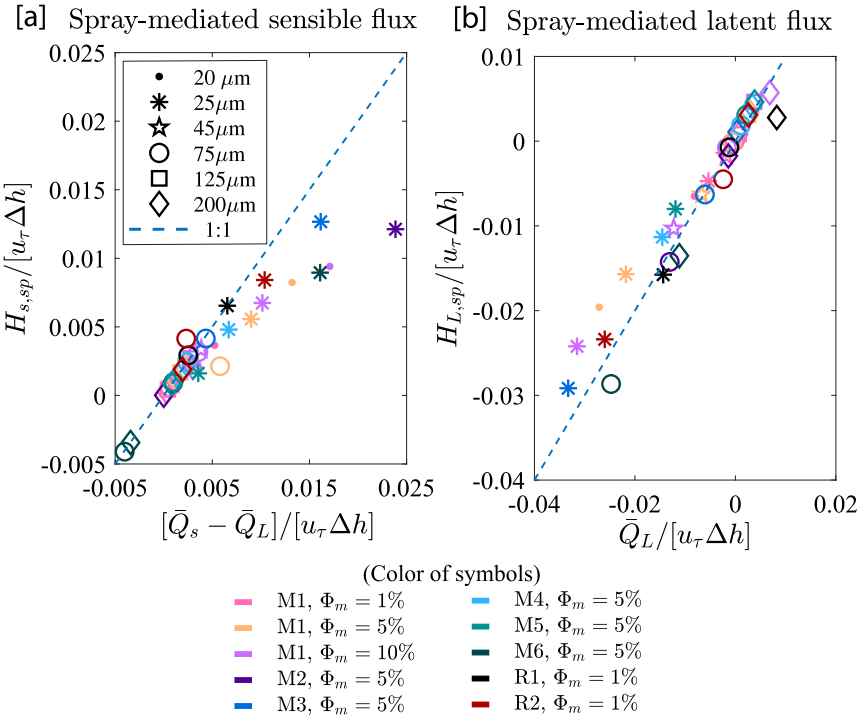

FIG. 2. Estimated spray-mediated heat fluxes vs DNS-computed results: (a) spray-mediated sensible heat flux ($H_{s,\mathrm{sp}}$ vs $\overline{Q}_s$) and (b) spray-mediated latent heat flux ($H_{L,\mathrm{sp}}$ vs $\overline{Q}_L$). The product of the friction velocity u_τ and the vertical enthalpy difference of the domain Δh is used to normalize heat fluxes.

Eqs. (2)–(4), which in A15's notation use $\alpha = \beta = 1$ and $\gamma = 0$ according to Eqs. (5)–(7). Thus for F94, the latent spray-mediated heat flux is approximated by the nominal flux $\overline{Q}_L$, and the sensible spray-mediated heat flux is expressed as the difference between the total and the latent fluxes, $\overline{Q}_s - \overline{Q}_L$. To test the estimates given by Eqs. (3) and (4), we plot in Fig. 2 the DNS-computed spray fluxes $H_{s,\mathrm{sp}}$ and $H_{L,\mathrm{sp}}$ against $\overline{Q}_s - \overline{Q}_L$ and $\overline{Q}_L$, respectively, where based on Eqs. (8) and (9) we calculate $\overline{Q}_s$ and $\overline{Q}_L$ from droplet statistics ΔT_p and Δm_p known from the DNS. Spray radii in the plot range from 20 to 200 μm, and we include all three Reynolds numbers and boundary conditions. We normalize the heat fluxes by the product of friction velocity u_τ and total enthalpy difference ($\Delta h = h_{\mathrm{bot}} - h_{\mathrm{top}}$) between the top and bottom boundaries.

Figure 2 shows that spray behaves differently as a function of droplet size. For example, in Fig. 2b for the latent heat flux $H_{L,\mathrm{sp}}$, 200-μm droplets provide a positive contribution of latent heat to the system ($H_{L,\mathrm{sp}} > 0$) although the amount is small. As radius decreases, the magnitude of $H_{L,\mathrm{sp}}$ increases, and spray actually extracts latent heat from the air when the bottom surface exhibits a warmer and more humid condition. However, both panels in Fig. 2 show that F94 has drawbacks of predicting heat fluxes of smaller droplets (25 μm or less), in particular for the sensible spray-mediated heat flux $H_{s,\mathrm{sp}}$, where deviations are observed for the smaller droplets (shown by asterisks and dots). Specifically, points beneath the reference line in Fig. 2a indicate an overprediction of spray-mediated sensible heat flux calculated by the F94 model for small droplets. Meanwhile, Fig. 2b suggests a slight underprediction of latent spray-mediated heat flux via the F94 model for small droplets, although this effect is smaller. Nevertheless, the different directions of deviations indicate an internal reallocation of sensible and latent spray-mediated heat flux due to spray evaporation/condensation, which is related to the cancellation and feedback effects documented in PR17. Thus, if the deviations for smaller droplets are due solely to the internal reallocation of sensible and latent heat fluxes, we would expect F94 to predict the total spray-mediated heat flux more accurately than its sensible/latent components.

Therefore, Fig. 3 plots the total spray-mediated heat flux as calculated by the DNS (H_{sp}; vertical axis) and the F94 model [Eq. (2); horizontal axis]. As seen in the figure, F94 indeed does predict the total spray-mediated heat flux fairly accurately, which confirms that the deviations in Fig. 2 are due to reallocation of sensible and

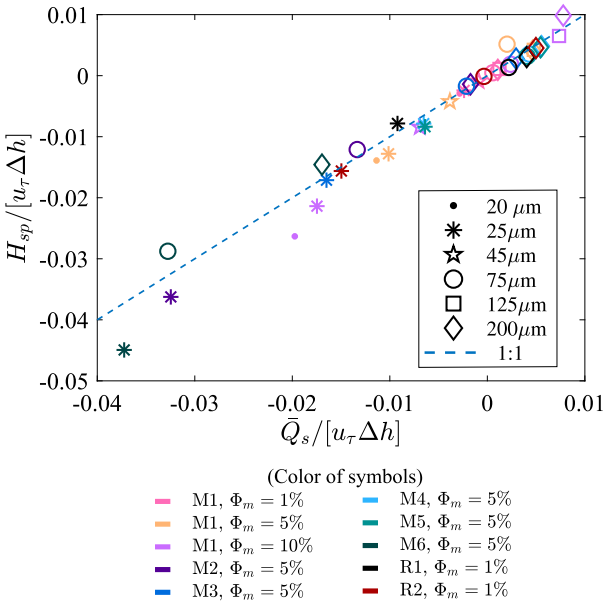

FIG. 3. DNS-computed spray-mediated total heat flux H_{sp} vs nominal sensible heat flux $\overline{Q}_s$, showing that spray-mediated heat fluxes are reflected in its internal energy change. Heat fluxes are normalized by the product of u_τ and Δh. Various simulations with different Re_τ, Φ_m, and size are denoted by color and marker in the legends. See Table 3 for simulation settings.

latent heat fluxes. In addition, the clustering around the reference lines in Fig. 3 confirms the assumption by F94 that the total heat exchanged with spray is reflected in its temperature change (via $\overline{Q}_s$). This is because the changes of droplet radius and temperature are separate processes occurring at disparate response time scales—see, for example, Fig. 1 in Andreas and Emanuel (2001).

In the above discussion, we verify that the F94 model works well at predicting total and latent spray-mediated heat fluxes when applying the known statistics of spray microphysics directly retrieved from DNS. Similar conclusions can be drawn for the A15 model. Based on Fig. 2, we can confirm that the coefficient α for latent flux $H_{L,\mathrm{sp}}$ in the A15 model [Eqs. (5) and (6)] is indeed $O(1)$. However, the value of β based on the DNS for the spray-mediated sensible heat flux is not as large as what the A15 model predicts. According to A15, $\beta = 15.15$, whereas the DNS results suggest that $\beta \approx 1$, as evidenced by symbols clustering near the reference line in Fig. 2a. Furthermore, to predict the spray-mediated $H_{s,\mathrm{sp}}$, we find that the feedback coefficient γ is negligible if we assume that $\alpha = 1$. Therefore, the implied values $\alpha = \beta = 1$ in the F94 model are a good approximation of the total spray-mediated heat flux given a correct estimate of spray microphysics (i.e., Δm_p and ΔT_p), and the A15 model may overestimate the sensible heat flux by an order of magnitude due to the large value of β. The question of whether a nonzero γ is required to describe interplay between spray-mediated and interfacial fluxes is considered next.

b. *The feedback effect of spray evaporation*

The above analysis demonstrates that one can obtain reasonably accurate predictions for the total spray-mediated flux H_{sp} with an accurate prediction of $\overline{Q}_L$ and $\overline{Q}_s$. However, it remains to be verified whether the spray-mediated fluxes can simply be added to the spray-free interfacial fluxes to yield the total heat flux. In the F94 model, the total heat flux is $H_T = H_{\mathrm{int}} + H_{\mathrm{sp}}$, which makes no attempt to account for any reductions in the interfacial flux due to the presence of the spray-mediated component. In contrast, the A15 model considers a feedback effect between the two, which is associated with the latent heat released from the spray by the γ parameter in Eq. (6). The parameter γ takes into account the fact that latent spray-mediated heat flux from the droplet phase can modify the corresponding interfacial flux, presumably by moistening the near-surface air and increasing the temperature gradient by evaporative cooling (e.g., when $\gamma > 0$). Since we calculate each term in Eq. (1) explicitly in DNS, we shift our focus to the total heat flux H_T and discuss whether the bulk models provide a reasonable estimate for the total heat flux as well.

We first evaluate whether one can add the spray-mediated heat fluxes to the interfacial heat fluxes estimated from spray-free conditions as F94 suggests. To test this assumption, we compute an unladen case (with subscripts 0) from DNS in which the total heat flux consists solely of the interfacial flux $H_{\mathrm{int},0}$. Then, we add $H_{\mathrm{int},0}$ to the bulk estimate of the total spray-mediated flux H_{sp} by F94 via Eqs. (2) and (8) for the corresponding spray-laden cases, and we plug them into Eq. (1); that is, $H_T = H_{\mathrm{int},0} + \overline{Q}_s$.

Figure 4 shows that the DNS-calculated H_T versus the estimates given by the F94 model do not always agree. In particular, the estimates for smaller droplets ($r_p < 25\ \mu$m) can deviate by up to 120% from the corresponding DNS-calculated values, although the predictions of F94 are more acceptable for larger droplets ($r_p > 75\ \mu$m) especially with warmer bottom surface. Thus, according to Fig. 4, how well F94 predicts the H_T depends on the droplet size.

Along the lines of A15, we assume the error in Fig. 4 is due to the feedback effect between spray and interfacial fluxes. We test this assumption by defining the change of interfacial flux ΔH_{int} from the unladen case after loading spray droplets:

$$\Delta H_{\mathrm{int}} = H_T - (H_{\mathrm{sp}} + H_{\mathrm{int},0}). \tag{17}$$

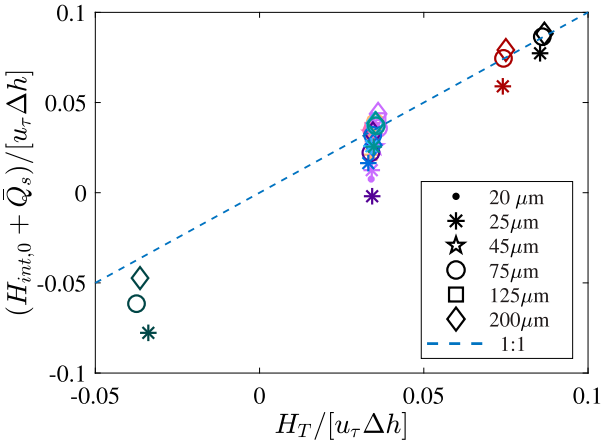

FIG. 4. DNS-computed total heat flux H_T vs the estimated total heat flux (H_{sp} + $H_{int,0}$) by adding the DNS-computed spray-mediated flux with the corresponding unladen total interfacial heat flux. The heat fluxes are normalized by $u_\tau\Delta h$. Colors of the symbols and marker styles in the legends match Fig. 3.

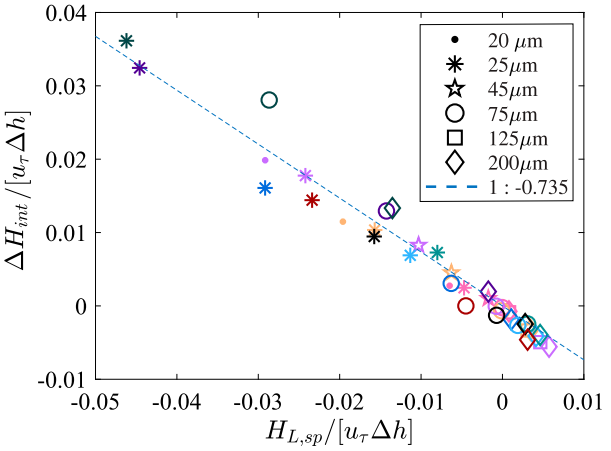

FIG. 5. Modification of total interfacial heat flux H_{int} vs nominal latent heat flux $\overline{Q}_L$, showing that evaporation of spray induces a modification of the total interfacial heat flux. Colors of symbols and marker styles in the legends match Fig. 3.

If the feedback is negligible, the ΔH_{int} should be approximately zero. Otherwise, ΔH_{int} in Eq. (17) quantifies the net feedback between spray and interfacial heat fluxes that is missing in bulk models.

In Fig. 5, we plot ΔH_{int} versus the DNS-calculated spray-mediated latent heat flux $H_{L,sp}$. Interestingly, comparing the net feedback ΔH_{int} with $H_{L,sp}$ in Fig. 5, we find that ΔH_{int} is *inversely* proportional to $H_{L,sp}$. The negative linear trend in Fig. 5 is in contrast to the feedback effect assumed by A15, which indicates a negative feedback effect induced by spray. Hence the interfacial heat flux will adjust itself to attenuate the influence from spray evaporation rather than being enhanced by spray droplets. We can describe this linear relationship as

$$\Delta H_{int} = \gamma H_{L,sp}, \tag{18}$$

where the coefficient is determined as $\gamma = -0.7349$ with $R^2 = 0.9895$ by linear regression.

Because we have shown that the bulk estimates of spray-mediated latent heat flux $\overline{Q}_L$ agree reasonably well with the DNS-calculated $H_{L,sp}$ in Fig. 2b, we arrive at an approximation for the total heat flux:

$$H_T \approx H_{int,0} + \overline{Q}_s + \gamma\overline{Q}_L, \tag{19}$$

where $\gamma = -0.7349$, $H_{int,0}$ is the unladen total interfacial heat flux, and $\overline{Q}_s$ is the approximation of the total spray-mediated heat flux H_{sp} shown in Fig. 3.

With the correction of the negative feedback term from DNS results, we plot the two sides of Eq. (19) using bulk estimates of spray-mediated heat fluxes in Fig. 6. It is obvious that the errors are significantly reduced to a range around 5% compared to Fig. 4, especially for smaller droplets. Therefore, the negative feedback term ($\gamma < 0$) in Eq. (19) suggests that both F94 and A15 models can overestimate the influence of spray on the total heat flux when there is a substantial amount of latent heat flux released by spray, although the F94 model works when the spray-mediated latent flux $\overline{Q}_L$ is small. Moreover, the A15 model can further overestimate it by imposing a positive feedback term ($\gamma > 0$). We briefly summarize the main comparisons of the bulk algorithms with DNS in Table 5.

Based on Eq. (19), one can see that the quality of estimating $\overline{Q}_s$ and $\overline{Q}_L$ determines the accuracy of the final prediction of H_T, and $\overline{Q}_s$ and $\overline{Q}_L$ are calculated via spray's microphysics (i.e., ΔT_p and Δr_p). In the above discussion, we directly apply ΔT_p and Δr_p from our DNS model to the bulk algorithms, so the next step is to examine the assumptions behind how bulk models quantify $\overline{Q}_s$ and $\overline{Q}_L$.

c. *Spray evaporation in turbulent air and its temporal dependence*

In bulk models, the evaporation for all spray droplets occurs with an assumed constant ambient condition (e.g., the 10-m temperature and RH) that is usually drier and cooler than the lower part of the ASI, as we have shown in section 2b. In this section, we use the Lagrangian statistics of spray droplets in the DNS to investigate the characteristics of spray evaporation, specifically to test the behavior of ΔT_p and Δr_p and compare with solutions given by constant ambient conditions as per bulk models.

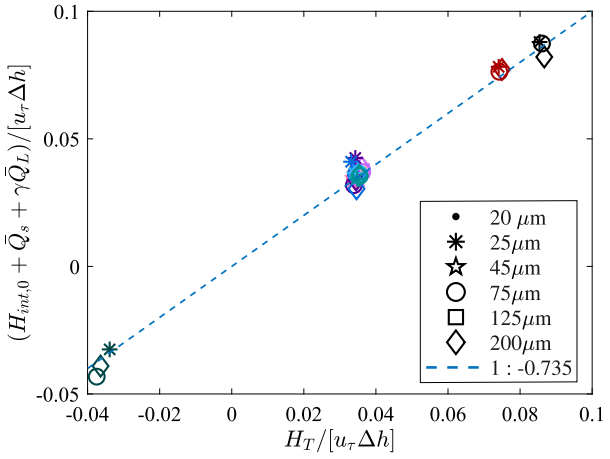

FIG. 6. DNS-computed H_T vs the estimated total heat flux by Eq. (19) with a negative feedback term from the spray-mediated $\overline{Q}_L$. Colors of symbols and marker styles in the legends match Fig. 3.

1) INFLUENCE OF SPRAY TIME SCALES

We have illustrated three time scales involved in spray evaporation in turbulent air in Fig. 1: the residence time t_L, and the thermodynamic evolution time scales, τ_T for temperature and τ_r for radius. In this section, we will discuss how these time scales are associated with the relationship between the net differences ΔT_p and Δr_p with t_L. In Fig. 7, we plot the joint probability density function (JPDF) of these quantities for droplets with $r_p = 25$, 75, and 200 μm for $\mathrm{Re}_\tau = 1500$. Since all spray droplets in the DNS are initialized with same temperature and radius, the JPDFs in Fig. 7 are equivalent to the distributions of the reentrance temperature and radius, which varies on spray initial size.

As seen in Fig. 7, the maximum of the residence time t_L (shown in vertical axes) decreases as the initial droplet size increases. This phenomenon is because both the settling velocity and inertial effects increase with r_p. We also find two qualitatively distinct types of distribution of spray temperature and radius change with t_L observed in Fig. 7. The first is a strong correlation between ΔT_p or Δr_p and t_L (e.g., Figs. 7b,d,e,f); that is, the longer the residence time is, the greater is the magnitude in the change of spray temperature or radius. This relationship is similar in principle to what A15 assumes. The second type of distribution features a high-density area at small values of t_L and a much weaker correlation between ΔT_p and t_L (e.g., Fig. 7a), while Fig. 7c appears to be a transition between the two. This is similar in principle to F94's assumption that spray immediately adjusts to the ambient air temperature, and it is observed that the high-density area is independent of residence time (parallel to the vertical axis). Therefore, only assuming one temporal relationship for spray temperature change does not appear to cover all scenarios for various spray sizes, and the various time scales associated with a droplet's thermodynamic evolution and lifetime should be carefully considered when parameterizing their radius and temperature change for use in bulk models.

TABLE 5. Coefficients of heat transfer of bulk models and DNS results, given $H_{L,\mathrm{sp}} = \alpha\overline{Q}_s$, $H_{s,\mathrm{sp}} = \beta\overline{Q}_s - (\alpha - \gamma)\overline{Q}_s$, and $H_T = H_{\mathrm{int}} + \beta\overline{Q}_s + \gamma\overline{Q}_L$.

	F94	A15	DNS
α	1	2.46	1
β	1	15.15	1
γ	0	1.77	−0.71

How ΔT_p and Δr_p are associated with t_L depends on their time scales τ_T and τ_r. Andreas (2005) defines τ_T as the time required for changing to a factor of $1 - e^{-1}$ of the initial temperature. Thus, τ_T is proportional to r_p^2 since it is based on the exposed surface area for heat transfer. Based on Eqs. (15) and (16), one can notice that temperature and radius change are strongly correlated with time within τ_T or τ_r respectively (Andreas 1992; Veron 2015). For example, given the top boundary condition of M1 in Table 3, τ_T for 25-μm droplets is 7.3 ms, and τ_T is 47 ms for 200 μm. The response time for radius τ_r is defined either by the e-folding time (used in the A15 model) or a linear decay rate (e.g., Lewis and Schwartz 2004) and is also proportional to r_p^2. Thus, Fig. 7a shows an increased probability density concentrated at a specific temperature for all t_L, suggesting that the near-surface environment would play a dominant role governing the reentrance temperature regardless of the residence time. In this scenario, t_L is not a good indicator for ΔT_p.

Because τ_r is greater than τ_T by three orders of magnitude (Andreas 2005; Veron 2015), radius change with the ambient air is a much slower process than temperature adjustment. Thus, we expect radius to present a strong correlation for a wide range of t_L because $\tau_r > t_L$ for most droplets. For this reason, we select the shorter time scale τ_T to nondimensionalize t_L and define a nondimensional time scale as

$$\tilde{t}_L = t_L/\tau_T. \tag{20}$$

By definition, if $\tilde{t}_L \leq O(1)$, the limiting time scale for the evaporation is the residence time t_L, and spray cannot finish the initial temperature adjustment and is less likely to experience a wide range of temperature and humidity, so ΔT_p should retain a strong correlation with t_L. However, when $\tilde{t}_L > O(1)$, the limiting time scale is τ_T and spray tends to establish a new equilibrium with the ambient air.

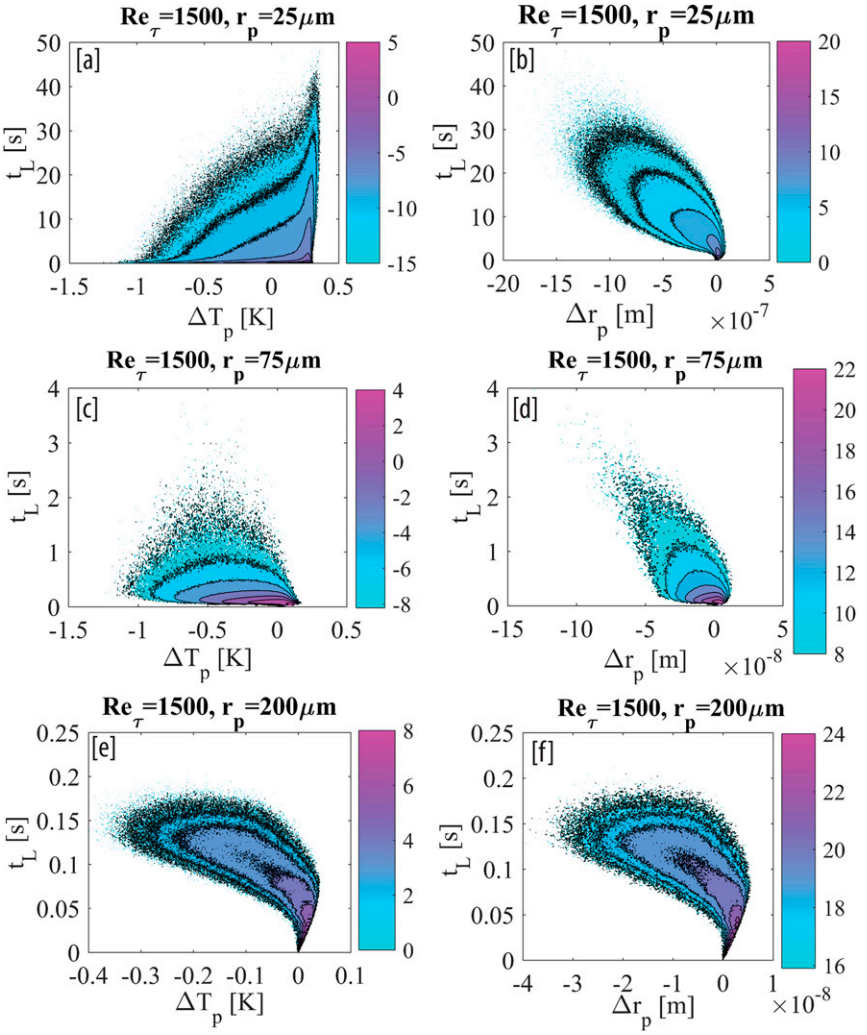

FIG. 7. JPDFs of t_L and (left) droplet temperature change ΔT_p and (right) radius change Δr_p at $\mathrm{Re}_\tau = 1500$. Three radii are presented: (a),(b) 25; (c),(d) 75; and (e),(f) 200 μm. Color bars represent the density of the JPDFs in log scale.

Thus, if $\tilde{t}_L > O(1)$, using its initial conditions would lead errors in estimating the spray's returning temperature based on its residence time given a stationary ambient condition, because spray will "forget" its initial state. For example, when F94 assumes that spray instantaneously adjusts to the air temperature at the representative location (the 10-m condition), we would expect a peak of ΔT_p which is always clustered at negative values due to evaporative cooling. Figure 7a shows, however, that ΔT_p in the high-density regions of the JPDFs for small droplets (especially for 25 μm) is positive; that is, the spray is warmed due to condensation effect near surface. Therefore, given a different time scale balance, a model should distinguish the parameterizations of spray evaporation based on $\tilde{t}_L$.

As r_p increases, the ratio $\tilde{t}_L$ decreases rapidly because τ_T increases as r_p^2 (as noted above) while t_L decreases as a result of an increased settling velocity and higher inertia. This suggests a sharp border between the high- and low-correlation scenarios, possibly simplifying proper modeling strategies.

2) THE AMBIENT CONDITIONS OF SPRAY EVAPORATION

While the JPDFs in Fig. 7 show two distinct types of relationship between t_L and ΔT_p or Δr_p, bulk models still require specifications of the representative ambient conditions to predict the reentrance radius and temperature accurately.

To further quantify the relationship between spray evaporation against its residence time, in Figs. 8 and 9

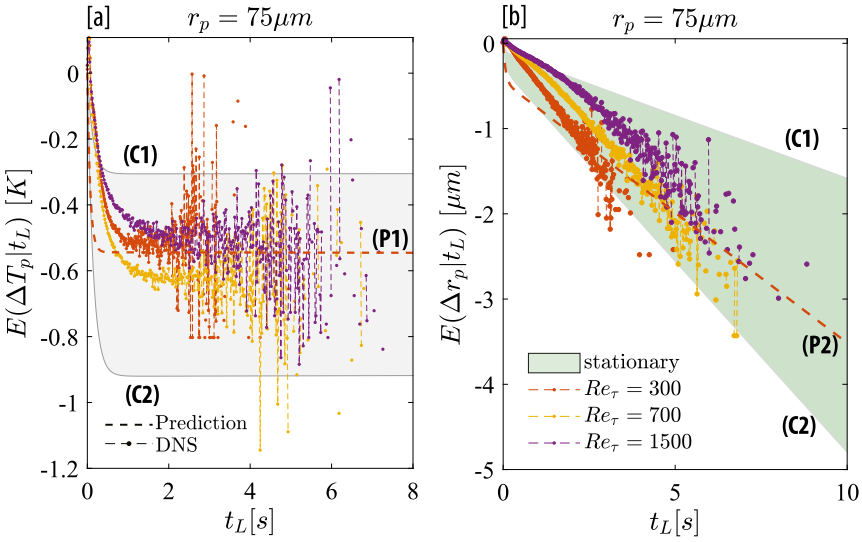

FIG. 8. Conditional mean of (a) ΔT_p (K) and (b) Δr_p (μm) given t_L (s) for 75-μm spray droplets. Shaded areas represent possible solutions of stationary evaporation (gray for ΔT_p and green for Δr_p) with limits from two assumed constant ambient conditions: C1 is RH = 97% and T_a = 27.8°C, and C2 is RH = 95.5% and T_a = 27.4°C. Also included are predictions using Eq. (21) for specifying representative ambient conditions: P1 is RH = 98.48% and T_a = 27.35°C, and P2 is RH = 96.19% and T_a = 26.85°C.

we plot the conditional mean (the expected value) of temperature and radius change given a residence time, $E(\Delta T_p|t_L)$ and $E(\Delta r_p|t_L)$, for varying Re_τ and r_p. We then compare the result with solutions which would have been retrieved from bulk models assuming a constant background ambient temperature and humidity (usually cooler and drier than the bottom surface). The idealized radius and temperature change with constant ambient background are given as curves "C1"–"C4" in the figures for different ambient conditions, with shading to represent conditions in between. Thus, in Figs. 8 and 9, if ΔT_p and Δr_p given the residence time are well predicted by the bulk models, we would see them follow the solutions of spray evaporation given stationary ambient conditions.

In some scenarios, the statistical behavior of spray droplets in DNS agrees with what bulk models assume. For example, as seen in Fig. 8b, the evolution of radius change Δr_p with lifetime is linear for almost all Re_τ, which is qualitatively expected when assuming constant background conditions. This would indicate that the turbulent fluctuations felt by the droplets in the DNS in this scenario are substantially filtered out as $\tilde{t}_L < O(1)$. In other words, it is feasible find a possible single ambient condition that the droplets have experienced to characterize spray's radius change. Similarly, we also notice that the temporal evolution of ΔT_p in Fig. 8a is in the range of possible steady-state solutions for spray droplets, at least for 75-μm droplets since $\tilde{t}_L$ is $O(1)$ (curves lie within the gray shaded area).

On the other hand, droplets with $\tilde{t}_L > O(1)$ have a different story (e.g., $\tilde{t}_L = 10.52$ for 25-μm droplets), as seen in Fig. 9. The ambient conditions used for estimating the change in radius (C3 and C4) cannot apply to its temperature (C1 and C2), although the conditional mean ΔT_p mostly follows some other stationary ambient conditions. In Fig. 9a, the condition C1 is the wet-bulb temperature at the bottom boundary, and C2 is the condition very close to the bottom boundary (RH = 98%). Neither of these causes spray to adjust to a cooler and drier ambient condition (resulting in negative ΔT_p) as F94 or A15 would expect. Instead, Fig. 9a shows a positive mean ΔT_p, indicating that condensation occurs on these droplets (also shown in Figs. 2 and 3). This phenomenon is because of the immediate response of the droplet to the local ambient conditions before impacting the lower surface. Even though some spray may have spent most of its lifetime away from the bottom surface, its reentrance temperature is predominately determined by the local condition due to the small τ_T (i.e., $\tilde{t}_L > 1$). Therefore, the selection of ambient condition for assuming a constant background needs to incorporate the limiting time scale.

To summarize, our DNS results suggest that the balance of residence time and other time scales modifies the selection of representative ambient conditions when mean gradients of air temperature and humidity are present above the ASI. We observe drawbacks in both F94 and A15 in this regard, especially in predicting the

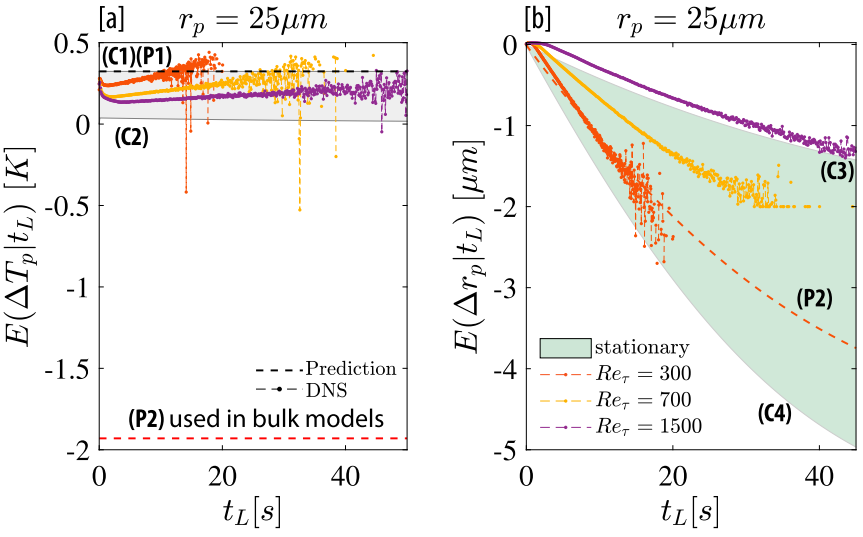

FIG. 9. Conditional mean (expectation) and predictions of (a) ΔT_p (K) and (b) Δr_p (μm) given t_L (s) for 25-μm spray droplets. The predictions (dashed lines) with equivalent ambient conditions are given by Eq. (21). The ambient conditions used for temperature are different from radius: C1 and P1 are the quasi-equilibrium evaporation temperature of the spray at RH = 100% and T_a = 28°C, C2 is RH = 98% and T_a = 28°C, C3 is RH = 98% and T_a = 27.8°C, C4 is RH = 95% and T_a = 27.4°C, and P2 is RH = 95.74% and T_a = 26.35°C.

reentrance temperature. However, the results do not necessarily exclude the possibility of assuming stationary ambient conditions within bulk models. What is needed is a more accurate specification of these assumed conditions (i.e., not simply the 10-m temperature and humidity).

Nevertheless, the question of how to specify this condition remains unanswered in real systems, and there are several necessary parameters of fluid and spray to consider. For example, as t_L increases, droplets with longer residence time experience slightly lower humidity as they are transported to a drier environment during their lifetime. Also, as Re_τ increases in our simulations, the gradient of background temperature and humidity changes. Thus, the change in Δr_p with t_L behaves as though an assumed background ambient condition were becoming more humid. For example in Figs. 8b and 9b, Δr_p for $\mathrm{Re}_\tau = 300$ is nearer the C2 (or C4) line at 95% RH while $\mathrm{Re}_\tau = 1500$ is nearer the C1 (or C4) line at 97%.

3) A TENTATIVE ESTIMATE OF THE EQUIVALENT AMBIENT CONDITION

Here we propose a simple, tentative estimate for these effective ambient conditions based on our DNS results. For heavy droplets (e.g., large spume droplets), spray's evaporation is usually limited by the residence time [$\tilde{t}_L < O(1)$], so both radius and temperature retain their correlation to the initial condition. Thus, we would assume the equivalent ambient conditions sit beneath the so-called spray layer $z \in (0, \delta_{\mathrm{spray}})$, defined as the maximum height that spray can reach (usually where spray concentrations are assumed to be uniform with height). In our DNS model, when spray exhibits inertial motions, $\delta_{\mathrm{spray}} = \delta_{\mathrm{inj}}$ is the maximum height that spray could reach without turbulent transport (shown in Table 4).

As $\tilde{t}_L$ increases for smaller spray droplets, δ_{spray} grows as droplets are transported more easily by turbulence across, and it eventually reaches $\delta_{\mathrm{spray}} = \delta$; that is, spray is distributed evenly across the domain (or perhaps the surface layer in real systems). Meanwhile, the surface conditions become more dominant as τ_T decreases. Therefore, the assumed location to extract the equivalent ambient condition needs to be a function of the limiting time scales, τ_T or τ_r. Otherwise, it would lead to inaccurate predictions of ΔT_p and Δr_p.

To improve this issue, we assume that spray droplets travel with a mean vertical settling velocity w_s, leading to the following expression for the height z_{evap} at which to extract the mean ambient conditions:

$$z_{\mathrm{evap},\phi} = 0.5 \min(\delta_{\mathrm{spray}}, w_s \tau_\phi), \tag{21}$$

where δ_{spray} is the height of the spray layer (when $\tilde{t}_L \ll 1$, it is assumed to be the height of the domain of interest), and τ_ϕ represents time scales for $\phi = r_p$ or T_p.

Then, the constant ambient conditions for air temperature and relative humidity to be used in the bulk models would be $T_a(z_{\text{evap},\phi})$ and $\text{RH}_a(z_{\text{evap},\phi})$, respectively.

For instance, we plot solutions based on the ambient condition predicted by Eq. (21) in Figs. 8 and 9 ("P1" for ΔT_p and "P2" for Δr_p in both figures), where we assume $z_{\text{evap},T} = 0$ and $z_{\text{evap},r} = 0.5\delta$ for 25-μm droplets and $z_{\text{evap},T} = 0.25\delta_{\text{inj}}$ and $z_{\text{evap},r} = 0.3\delta$ for 75-μm droplets. Although this estimation is only based on the hypothesis of the one-way coupling, we find that Eq. (21) overall provides a reasonable ambient condition for both cases and can significantly improve the error for ΔT_p (hence $\overline{Q}_s$) for the smaller spray with $\tilde{t}_L > O(1)$ than the conventional assumption.

d. *The importance of spray time scales on estimating spray feedback*

Different treatments of spray heat flux in bulk models cause significant differences in predicting the influence of the spray and thus the total heat flux. For example, when applying both F94 and the model of Andreas and Decosmo (1999) (a predecessor of the A15 model with same framework) to hurricane models (Wang et al. 2001), it is reported that the F94 model results in an increase by 8% of the intensity of the tropical cyclone, while A15 gives an increase by 25% and generates a physically unrealistic near-core environment. Previous discussions suggest that spray time scales are the key to accurately quantify the spray-mediated fluxes. Thus, in this section, we revisit the bulk estimations of total heat flux H_T and discuss the influence of spray time scales on estimating spray feedback.

We have shown in PR17 that two types of cancellation were identified in a turbulent system with evaporating spray droplets: one between spray-mediated sensible and latent heat fluxes, and the other between spray-mediated and turbulent (i.e., interfacial) heat fluxes. These cancellation effects prevent the spray droplets from enhancing the total heat flux without constraint. However, in their bulk models, F94 does not include an explicit form of the feedback effect on the interfacial heat flux, whereas A15 predicts this feedback effect as positive by stating that $\gamma > 0$ as a result of the assumption that spray cools the surface air. We have mentioned that both formulations would overestimate the influence of spray droplets.

Because spray evaporation induces a change in the total heat flux H_T, we define the change of total heat flux ΔH_T as the difference between the spray-laden and unladen cases: $\Delta H_T = H_T - H_{T,0}$. With bulk estimates, we can connect ΔH_T with the net change of spray's temperature and radius directly. Combining this with Eqs. (3) and (4), one gets

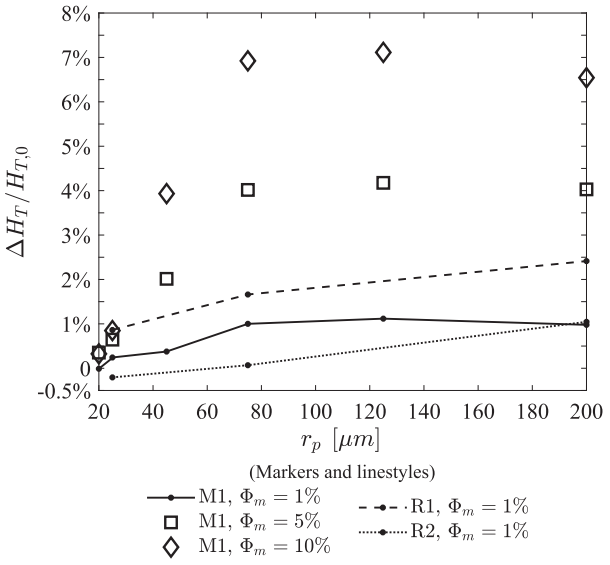

FIG. 10. Modification of H_T of different initial spray radii r_p relative to the no-spray scenario for each Re_τ with the same boundary conditions as indicated in Table 3. Here, M1 has $\text{Re}_\tau = 300$, R1 has $\text{Re}_\tau = 700$, and R2 has $\text{Re}_\tau = 1500$; markers specify the spray mass fraction.

$$\Delta H_T \approx \overline{Q}_s + \gamma \overline{Q}_L, \tag{22}$$

with $\gamma < 0$, which relates ΔH_T to the nominal spray-mediated heat fluxes, $\overline{Q}_s$ and $\overline{Q}_L$. Since $\overline{Q}_s$ and $\overline{Q}_L$ are defined as proportional to ΔT_p and Δr_p^3, ΔH_T can be approximated as a linear function of ΔT_p and Δr_p^3 given a specific spray generation rate F. Therefore in principle one can predict the change of total heat flux based on the temperature and radius of the reentering spray. Based on the previous discussion on ΔT_p and Δr_p, we have two major scenarios for spray feedback effects.

The first scenario occurs for spray with $r_p > 50$ μm when spray evaporation is limited by its residence time (e.g., spume drops); that is, $\tilde{t}_L \ll 1$, where we expect $\overline{Q}_s > \overline{Q}_L > 0$ as the radius change is small (cf. Fig. 8), and thus $\Delta H_T > 0$. Note in Fig. 3 that we confirm that $\overline{Q}_s$ is a good estimate for the total spray-mediated heat flux H_{sp}, so we expect $\overline{Q}_s > \overline{Q}_L$. Therefore, spray in this regime enhances H_T, and the enhancement grows with the generation rate.

In Fig. 10, we plot the relative modification of total heat flux ($\Delta H_T/H_{T,0}$) for different Re_τ and Φ_m with respect to droplet size r_p. We observe a low sensitivity of ΔH_T to Re_τ but a fairly high sensitivity to Φ_m, and the enhancements of ΔH_T by 75- and 200-μm droplets in Fig. 10 demonstrate the potential of the enhancement of H_T by spray with $\tilde{t}_L \ll 1$, especially under high spray-generation rate F. In addition, $-\gamma \overline{Q}_L$ is very small because Δr_p is small, so the interfacial feedback is insignificant in

this scenario. Thus, the framework that F94 presents (with no negative feedback term) can physically represent H_T for spray with $\tilde{t}_L \ll 1$.

The second scenario occurs when the residence time no longer limits spray's temperature adjustment; that is, $\tilde{t}_L > 1$. Figure 9 indicates that $\overline{Q}_L < \overline{Q}_s < 0$ at the bottom surface; that is, small droplets condense near the surface (cf. Fig. 7), which is not considered in most bulk and 1D models. In addition, the combination of $\overline{Q}_s$ and $\overline{Q}_L$ makes $\Delta H_T/H_{T,0} \leq 0(0.01)$ as one can see in Fig. 10. We also observe that as the mass fraction increases by a factor of 10 (solid lines vs diamonds in Fig. 10), 25-μm droplets show an overall insensitivity to Φ_m. Based on Eqs. (9) and (8), the insensitivity on mass fraction indicates that $\overline{Q}_s$ and $\overline{Q}_L$ would be less dependent on the spray generation rate in real systems. Since there is a weak dependence on Re_τ for ΔH_T in Fig. 10, we argue that the dominant influence on $\overline{Q}_L$ and $\overline{Q}_s$ for 25-μm-or-smaller droplets is the local boundary condition when spray reenters the bottom surface. Therefore, the discrepancy of the spray modification on the total heat flux between DNS and bulk models comes from the direction of the latent heat flux at the bottom surface.

Although the condensation effect that is determined by the boundary condition sounds counterintuitive, the fact that small droplets can condense ($\overline{Q}_L < 0$ and thus $H_{L,\mathrm{sp}} < 0$) near the bottom surface does not conflict with their potential to evaporate hence increase the local humidity and decrease evaporation away from the surface. In fact, the two phenomena are consistent if one can interpret the time scales of spray properly per their corresponding ambient conditions, although we only focus on the bulk models at the bottom surface in the current study.

For the lower part of the domain ($z \in [0, 0.125\delta]$), we plot in Fig. 11 the averaged spray-mediated sensible and latent heat fluxes computed by DNS: $H_{s,\mathrm{sp}}$ and $H_{L,\mathrm{sp}}$. The DNS heat fluxes are normalized by the product of friction velocity u_τ and total enthalpy difference Δh ($=h_{\mathrm{bot}} - h_{\mathrm{top}}$) between the top and bottom boundaries, respectively. The positive spray-mediated latent heat flux $H_{L,\mathrm{sp}}$ in Fig. 11 represents an upward latent heat flux from spray evaporation. For the sensible heat flux $H_{s,\mathrm{sp}}$, we find that spray with $r_p < O(50\,\mu\mathrm{m})$ has a sensible heat flux $H_{s,\mathrm{sp}}$ with opposite sign to the latent flux, which indicates that the evaporative cooling effect cancels out the latent heat flux released from the spray. This leads to a smaller estimation of $\overline{Q}_s$ than the estimate without considering cancellation and thus yields the limited enhancement in Fig. 10. Spray with $r_p > O(50\ \mu\mathrm{m})$ has positive $H_{s,\mathrm{sp}}$ and cannot cancel $H_{L,\mathrm{sp}}$, which results in a larger value of $\overline{Q}_s$ and thus has a net positive contribution to the total heat flux that is discussed in sect. 3c.

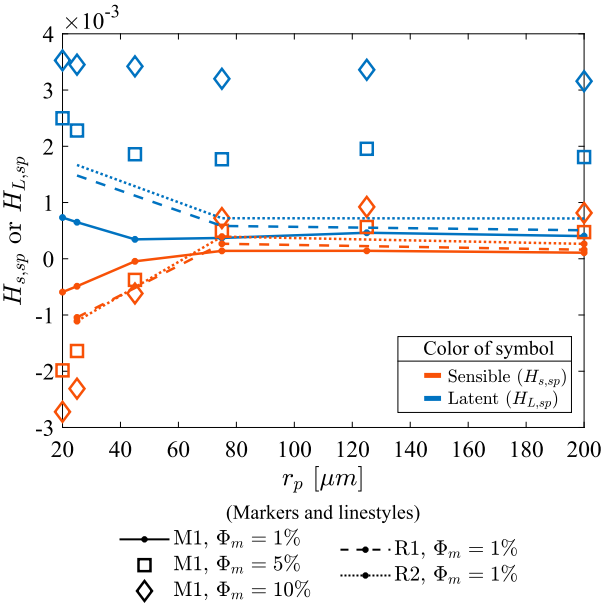

FIG. 11. Spray-mediated sensible ($H_{s,\mathrm{sp}}$) and latent ($H_{L,\mathrm{sp}}$) fluxes averaged in the spray layer $z \in [0, \delta_{\mathrm{inj}}]$. The heat fluxes are normalized by $u_\tau \Delta h$. Colors specify the sensible or latent components, and line and marker styles are as in Fig. 10.

Whether the spray exhibits this cancellation of spray-mediated fluxes depends on its time scales. The quick adjustment to the fluctuating temperature and humidity by spray allows the spray to reach the equilibrium temperature at a highly localized position (e.g., PR17). Here, as we can see from Fig. 11, cancellation occurs when $\tilde{t}_L > O(1)$ when spray is away from surface. At the bottom surface, the cancellation effect still occurs as we have seen in Fig. 2 since $H_{s,\mathrm{sp}}$ and $H_{L,\mathrm{sp}}$ have different signs. Therefore, from both perspectives, the cancellation effect or the condensation at the surface, show that bulk model can overestimate the spray-mediated heat fluxes.

To summarize, time scales of spray play an important role in predicting the total heat flux besides spray-mediated heat fluxes based on Eq. (22), which needs be incorporated in bulk models. As a result, the bulk estimation could have better parameterizations of ΔT_p and Δr_p, and the influence of spray, in particular given its different dependence on $\tilde{t}_L$, can be better understood.

4. Conclusions

In this study, we investigate how total heat flux responds to sea-spray via high-resolution Eulerian–Lagrangian simulations, where we use DNS to represent turbulent airflow in the lower atmospheric boundary layer at the air–sea interface with neutral stability. We apply the principles from air–sea bulk models that estimate total

heat transfer from the water surface and compare to our DNS results. Under our current idealized settings, we find spray might not necessarily enhance the total heat flux in turbulent flow with constant vertical heat flux. Also, the current study suggests the importance of spray time scales on parameterization of spray-mediated heat fluxes. We find a nonmonotonic relationship between spray's enhancement to the total heat flux and its residence time so that models like F94 and A15 can overestimate the influence of spray droplets for several reasons.

First, previous understanding of the feedback mechanisms of spray is not complete. Our DNS results suggest that the total heat flux cannot always be expressed as the sum of an interfacial and a spray mediated component directly, especially for droplets with small size (e.g., $r_p \leq 25$ μm). We find an additional negative feedback mechanism for total interfacial heat flux that is proportional to the spray-mediated heat flux at the surface [negative γ term in Eq. (17)]. This negative feedback effect limits the overall influence of spray regarding the total heat flux from the water surface, which is not included in either F94 or A15. In particular, the A15 model argues that spray-mediated latent heat flux would insert positive feedback to the total heat flux, which is not observed in our DNS results (see Table 5 for a comparison). Therefore, we would suggest further implementation on the negative feedback effects and investigations on its tuning coefficient for bulk models in practical use.

Second, inaccurate estimates of spray evaporation could also cause bulk models to fail to capture the cancellation effect between spray sensible and latent heat flux for smaller droplets. The failure is due to the different time scales involved in droplet evaporation when evaluating the spray evaporation via assumed-stationary ambient solutions, particularly when the droplet experiences a wide range of environmental conditions during its lifetime.

We find that the balance between the residence time and temperature response time of spray $\tilde{t}_L$ is a good indicator for determining whether a stationary ambient condition can be assumed for the droplet. When the residence time is longer than temperature time scales, $\tilde{t}_L > O(1)$, the reentrance temperature and radius of spray lose their correlation with the initial condition, and are determined by the local condition at the water surface. Therefore, the assumption that spray reenters the water surface with substantially decreased temperature (e.g., ones determined by 10-m conditions) would not apply and would introduce further overestimations to the spray-mediated sensible heat flux.

When the residence time is shorter than the correlation time scales of evaporation—that is, $\tilde{t}_L < O(1)$—spray retains a correlation with its initial condition. Therefore, ΔT_p and Δr_p follow the solutions with an assumed-stationary ambient condition like bulk models. As a consequence, spray in this regime has the potential to enhance the total heat flux, and the enhancement will be magnified by higher generation rates. However, the equivalent ambient condition is not uniform but is a function of spray time scales and is related to $\tilde{t}_L$. Since the spray temperature response time $\tau_T \approx 10^{-3}\tau_r$, further assumptions are required for bulk models to approximate the equivalent ambient for reentrance temperature and radius, and we propose an estimate of the equivalent ambient condition in Eq. (21) based on our DNS results.

Although our idealized study contains many simplifications regarding the surface processes (especially those associated with waves, such as wave breaking, droplet formation, etc.) and atmospheric variability, this study provides clear evidence that the spray effects are dependent on their thermodynamic time scales, and highlights physical processes (e.g., feedback) that are not properly accounted for in bulk models. Therefore, given a reasonable assumption for residence times across all sizes of spray, one could potentially improve the prediction of the total heat flux via bulk models without further complicating the model itself.

Acknowledgments. We acknowledge support from the National Science Foundation (NSF) Grant AGS-1429921. The authors thank the Computing Research Center at the University of Notre Dame for computational support. The authors also acknowledge high-performance computing support from Yellowstone (UNDM0004), maintained by the Computational Information Systems Laboratory at the National Center for Atmospheric Research (NCAR). NCAR is supported by the NSF. With permission, the supporting data of the current study are available online (https://doi.org/10.7274/r0-f1pa-8037).

REFERENCES

Andreas, E. L, 1992: Sea spray and the turbulent air-sea heat fluxes. *J. Geophys. Res.*, **97**, 11 429–11 441, https://doi.org/10.1029/92JC00876.

——, 2005: Approximation formulas for the microphysical properties of saline droplets. *Atmos. Res.*, **75**, 323–345, https://doi.org/10.1016/j.atmosres.2005.02.001.

——, and J. Decosmo, 1999: Sea spray production and influence on air-sea heat and moisture fluxes over the open ocean. *Air-Sea Exchange: Physics, Chemistry and Dynamics*, Springer, 327–362, https://doi.org/10.1007/978-94-015-9291-8_13.

——, and K. A. Emanuel, 2001: Effects of sea spray on tropical cyclone intensity. *J. Atmos. Sci.*, **58**, 3741–3751, https://doi.org/10.1175/1520-0469(2001)058<3741:EOSSOT>2.0.CO;2.

——, J. B. Edson, E. C. Monahan, M. P. Rouault, and S. D. Smith, 1995: The spray contribution to net evaporation from the sea: A review of recent progress. *Bound.-Layer Meteor.*, **72**, 3–52, https://doi.org/10.1007/BF00712389.

——, L. Mahrt, and D. Vickers, 2015: An improved bulk air-sea surface flux algorithm, including spray-mediated transfer. *Quart. J. Roy. Meteor. Soc.*, **141**, 642–654, https://doi.org/10.1002/qj.2424.

Bao, J.-W., C. W. Fairall, S. a. Michelson, and L. Bianco, 2011: Parameterizations of sea-spray impact on the air-sea momentum and heat fluxes. *Mon. Wea. Rev.*, **139**, 3781–3797, https://doi.org/10.1175/MWR-D-11-00007.1.

Bell, M. M., M. T. Montgomery, and K. A. Emanuel, 2012: Air-sea enthalpy and momentum exchange at major hurricane wind speeds observed during CBLAST. *J. Atmos. Sci.*, **69**, 3197–3222, https://doi.org/10.1175/JAS-D-11-0276.1.

Bianco, L., J. W. Bao, C. W. Fairall, and S. A. Michelson, 2011: Impact of sea-spray on the atmospheric surface layer. *Bound.-Layer Meteor.*, **140**, 361–381, https://doi.org/10.1007/s10546-011-9617-1.

Clift, R., J. R. Grace, and M. E. Weber, 1978: *Bubbles, Drops, and Particles*. Academic Press, 400 pp.

DeCosmo, J., K. B. Katsaros, S. D. Smith, R. J. Anderson, W. A. Oost, K. Bumke, and H. Chadwick, 1996: Air-sea exchange of water vapor and sensible heat: The Humidity Exchange Over the Sea (HEXOS) results. *J. Geophys. Res. Oceans*, **101**, 12 001–12 016, https://doi.org/10.1029/95JC03796.

Drennan, W. M., J. A. Zhang, J. R. French, C. McCormick, and P. G. Black, 2007: Turbulent fluxes in the hurricane boundary layer. Part II: Latent heat flux. *J. Atmos. Sci.*, **64**, 1103–1115, https://doi.org/10.1175/JAS3889.1.

Druzhinin, O. A., Y. Troitskaya, and S. Zilitinkevich, 2018: The study of momentum, mass, and heat transfer in a droplet-laden turbulent airflow over a waved water surface by direct numerical simulation. *J. Geophys. Res. Oceans*, **123**, 8346–8365, https://doi.org/10.1029/2018JC014346.

Edson, J. B., and C. W. Fairall, 1994: Spray droplet modeling: 1. Lagrangian model simulation of the turbulent transport of evaporating droplets. *J. Geophys. Res.*, **99**, 25 295–25 311, https://doi.org/10.1029/94JC01883.

——, S. Anquetin, P. G. Mestayer, and J. F. Sini, 1996: Spray droplet modeling: 2. An interactive Eulerian-Lagrangian model of evaporating spray droplets. *J. Geophys. Res.*, **101**, 1279–1293, https://doi.org/10.1029/95JC03280.

Fairall, C. W., J. D. Kepert, and G. J. Holland, 1994: The effect of sea spray on surface energy transports over the ocean. *Global Atmos. and Ocean Syst.*, **2**, 121–142.

Helgans, B., and D. H. Richter, 2016: Turbulent latent and sensible heat flux in the presence of evaporative droplets. *Int. J. Multiph. Flow*, **78**, 1–11, https://doi.org/10.1016/j.ijmultiphaseflow.2015.09.010.

Jeong, D., B. K. Haus, and M. a. Donelan, 2012: Enthalpy transfer across the air-water interface in high winds including spray. *J. Atmos. Sci.*, **69**, 2733–2748, https://doi.org/10.1175/JAS-D-11-0260.1.

Kepert, J., C. Fairall, and J.-W. Bao, 1999: Modelling the interaction between the atmospheric boundary layer and evaporating sea spray droplets. *Air-Sea Exchange: Physics, Chemistry and Dynamics*, Springer, 363–409, https://doi.org/10.1007/978-94-015-9291-8_14.

Komori, S., K. Iwano, N. Takagaki, R. Onishi, R. Kurose, K. Takahashi, and N. Suzuki, 2018: Laboratory measurements of heat transfer and drag coefficients at extremely high wind speeds. *J. Phys. Oceanogr.*, **48**, 959–974, https://doi.org/10.1175/JPO-D-17-0243.1.

Lewis, E. R., and S. E. Schwartz, 2004: *Sea Salt Aerosol Production: Mechanisms, Methods, Measurements and Models. Geophys. Monogr.*, Vol. 152, Amer. Geophys. Union, 413 pp.

Lighthill, J., 1999: Ocean spray and the thermodynamics of tropical cyclones. *J. Eng. Math.*, **35**, 11–42, https://doi.org/10.1023/A:1004383430896.

Makin, V. K., 1998: Air-sea exchange of heat in the presence of wind waves and spray. *J. Geophys. Res.*, **103**, 1137–1152, https://doi.org/10.1029/97JC02908.

Mestayer, P., and C. Lefauconnier, 1988: Spray droplet generation, transport, and evaporation in a wind wave tunnel during the humidity exchange over the sea experiments in the simulation tunnel. *J. Geophys. Res.*, **93**, 572–586, https://doi.org/10.1029/JC093iC01p00572.

Mueller, J. A., and F. Veron, 2010: A Lagrangian stochastic model for sea-spray evaporation in the atmospheric marine boundary layer. *Bound.-Layer Meteor.*, **137**, 135–152, https://doi.org/10.1007/s10546-010-9520-1.

——, and ——, 2014a: Impact of sea spray on air-sea fluxes. Part I: Results from stochastic simulations of sea spray drops over the ocean. *J. Phys. Oceanogr.*, **44**, 2817–2834, https://doi.org/10.1175/JPO-D-13-0245.1.

——, and ——, 2014b: Impact of sea spray on air-sea fluxes. Part II: Feedback effects. *J. Phys. Oceanogr.*, **44**, 2835–2853, https://doi.org/10.1175/JPO-D-13-0246.1.

Onishi, R., H. Fuchigami, K. Matsuda, and K. Takahashi, 2016: Detailed cloud microphysics simulation for investigation into the impact of sea spray on air–sea heat flux. *Flow, Turbul. Combust.*, **97**, 1111–1125, https://doi.org/10.1007/s10494-016-9766-x.

Peng, T., and D. Richter, 2017: Influence of evaporating droplets in the turbulent marine atmospheric boundary layer. *Bound.-Layer Meteor.*, **165**, 497–518, https://doi.org/10.1007/s10546-017-0285-7.

Pruppacher, H. R., and J. D. Klett, 1996: *Microphysics of Clouds and Precipitation*. Atmospheric and Oceanographic Sciences Library, Vol. 18, Springer, 954 pp.

Ranz, W. E., and W. R. Marshall, 1952: Evaporation from drops: Parts I and II. *Chem. Eng. Prog.*, **48** (3), 141–147, 173–180.

Rastigejev, Y., and S. A. Suslov, 2016: Two-temperature non-equilibrium model of a marine boundary layer laden with evaporating ocean spray under high-wind conditions. *J. Phys. Oceanogr.*, **46**, 3083–3102, https://doi.org/10.1175/JPO-D-16-0039.1.

Richter, D. H., and D. P. Stern, 2014: Evidence of spray-mediated air-sea enthalpy flux within tropical cyclones. *Geophys. Res. Lett.*, **41**, 2997–3003, https://doi.org/10.1002/2014GL059746.

——, and P. P. Sullivan, 2014: The sea spray contribution to sensible heat flux. *J. Atmos. Sci.*, **71**, 640–654, https://doi.org/10.1175/JAS-D-13-0204.1.

Soloviev, A. V., R. Lukas, M. A. Donelan, B. A. Haus, and I. Ginis, 2014: The air–sea interface and surface stress under tropical cyclones. *Sci. Rep.*, **4**, 5306, https://doi.org/10.1038/srep05306.

Troitskaya, Y., O. Druzhinin, D. Kozlov, D. Sergeev, and S. Zilitinkevich, 2018a: The ''bag breakup'' spume droplet generation mechanism at high winds. Part II: Contribution to momentum and enthalpy transfer. *J. Phys. Oceanogr.*, **48**, 2189–2207, https://doi.org/10.1175/JPO-D-17-0105.1.

——, A. Kandaurov, O. Ermakova, D. Kozlov, D. Sergeev, and S. Zilitinkevich, 2018b: The ''bag breakup'' spume droplet

generation mechanism at high winds. Part I: Spray generation function. *J. Phys. Oceanogr.*, **48**, 2167–2188, https://doi.org/10.1175/JPO-D-17-0104.1.

Veron, F., 2015: Ocean spray. *Annu. Rev. Fluid Mech.*, **47**, 507–538, https://doi.org/10.1146/annurev-fluid-010814-014651.

Wang, C. S., and R. L. Street, 1978: Transfers across an air-water interface at high wind speeds: The effect of spray. *J. Geophys. Res.*, **83**, 2959–2969, https://doi.org/10.1029/JC083iC06p02959.

Wang, Y., J. D. Kepert, and G. J. Holland, 2001: The effect of sea spray evaporation on tropical cyclone boundary layer structure and intensity. *Mon. Wea. Rev.*, **129**, 2481–2500, https://doi.org/10.1175/1520-0493(2001)129<2481:TEOSSE>2.0.CO;2.

Zhang, J. A., P. G. Black, J. R. French, and W. M. Drennan, 2008: First direct measurements of enthalpy flux in the hurricane boundary layer: The CBLAST results. *Geophys. Res. Lett.*, **35**, L14813, https://doi.org/10.1029/2008GL034374.